Machinery & Energetics
Vol. 17, No. 2. 2026

Journal homepage:
https://technicalscience.com.ua/en

UDC 631.362:004.94
DOI: 10.31548/machinery/2.2026.1

ISSN 2663-1334
e-ISSN 2663-1342

Viktor Duhanets*
Doctor of Pedagogical Sciences, Professor
Higher Educational Institution "Podillia State University"
32316, 12 Shevchenko Str., Kamianets-Podilskyi, Ukraine
https://orcid.org/0000-0002-3383-5907

Oleksandr Hovorov
PhD in Technical Sciences, Senior Researcher
Higher Educational Institution "Podillia State University"
32316, 12 Shevchenko Str., Kamianets-Podilskyi, Ukraine
https://orcid.org/0000-0002-1645-1725

Vitaliy Pukas
PhD in Technical Sciences, Associate Professor
Higher Educational Institution "Podillia State University"
32316, 12 Shevchenko Str., Kamianets-Podilskyi, Ukraine
https://orcid.org/0000-0002-0083-7359

Analysis and optimisation of internal combustion engine cooling systems to improve thermal efficiency and operational reliability

Abstract. The study aimed to quantitatively evaluate and optimise the operation of internal combustion engine cooling systems with a view to improving their thermal efficiency and reliability. The methodology combined engine bench tests with measurements of temperature, coolant and fuel flow rates, heat flux calculations with uncertainty assessment following guidance on the expression of measurement uncertainty, computational fluid dynamics in a coupled "fluid-solid" formulation, analysis of the stress-strain state of the cylinder head, and investigation of the transient warm-up regime from 20 to 90°C. The study established that the modernised configurations ensured a 10-17% increase in heat flux under maximum load conditions, a 5-6% and 10-12% reduction in peak temperatures in critical pre-chamber zones, and an 18-22% and 30-35% reduction in internal temperature gradients. This was accompanied by a reduction in equivalent stresses of 18-22% and an increase in the safety factor from 1.45 to 1.87 in the most efficient configuration. In transient mode, the system with an electric drive pump reduced the time to reach operating temperature by 9-12% and reduced integral fuel consumption by 10-12%, whilst the split-loop configuration provided a stable reduction in these figures of 6-8% and 5-7% respectively. An analysis of specific fuel consumption during braking in standard steady-state conditions revealed no statistically significant deterioration in fuel economy for the upgraded systems. The integrated ranking showed that a system with separate circuits provides a balanced combination of reduced of maximum temperature, minimised temperature gradients and increased safety margin without compromising fuel efficiency, whilst an electric drive pump is appropriate for minimising warm-up time and fuel consumption during cold starts. The practical significance of the study is determined by the development of quantitatively substantiated criteria for selecting cooling system configurations and coolant flow control strategies for engineering departments to improve thermal reliability and durability of engines

Keywords: local temperature gradients; thermal stress state; equivalent stresses; safety factor; transient heating regime; integral fuel consumption

Article's History: Received: 12.01.2026; Revised: 09.04.2026; Accepted: 21.05.2026; Published: 29.05.2026.

Suggested Citation:
Duhanets, V., Hovorov, & Pukas, V. (2026). Analysis and optimisation of internal combustion engine cooling systems to improve thermal efficiency and operational reliability. *Machinery & Energetics,* 17(2), 7-21. doi: 10.31548/machinery/2.2026.1.

*Corresponding author (duhanetsviktor@hotmail.com)

INTRODUCTION

Improvements in the thermal efficiency and reliability of modern internal combustion engines depend directly on the cooling system's ability to consistently maintain optimal temperatures across a wide range of loads and operating speeds. Overheating of critical areas of the combustion chamber, cylinder head and cylinder block accelerates wear, increases the risk of knocking and failures, whilst excessive cooling increases losses and reduces fuel efficiency. Therefore, the cooling system is regarded not merely as an auxiliary heat dissipation circuit, but as a controlled thermal subsystem module that directly influences the engine's performance and efficiency indicators, enabling a simultaneous improvement in both engine efficiency and service life.

W. Li *et al.* (2020) established, using numerical modelling of cavitation in the pump of an internal combustion engine (ICE) cooling system, that the reliability of predicting cavitation characteristics is determined by the accuracy of the cavitation model and the adequacy of the simulation of the formation and development of vapour cavities in the flow path. It is shown that cavitation not only limits the hydraulic efficiency of the pump but also reduces the reliability of the cooling system due to pressure pulsations, noise and accelerated wear of working surfaces. The optimisation of the heat transfer circuit using Computational Fluid Dynamics (CFD) methods is demonstrated in the study by S. Qin *et al.* (2022), where, using the example of a diesel engine water jacket, a causal relationship was established between the channel configuration, flow structure and the formation of the wall temperature field. It is shown that a reduction in local temperature peaks is achieved by controlling the hydrodynamics within the jacket, whereas simply increasing the coolant flow rate does not guarantee a proportional improvement in heat dissipation.

In parallel with design solutions, the role of active thermal control has been strengthened: M. Turabimana *et al.* (2023) proposed an active cooling system with a thermostat based on a shape-memory alloy, which implements adaptive control through controlled changes in the circuit's flow capacity. It has been demonstrated that replacing passive thermostating with an active approach improves the accuracy of temperature maintenance during transient conditions and simultaneously reduces the risk of overheating and losses due to overcooling. Research by D. di Battista *et al.* (2026), conducted under real-world driving conditions, showed that the coolant control strategy determines the thermal state of the engine during operational dynamics. It was established that controlling the temperature and flow rate of the coolant affects not only the intensity of warm-up and total heat losses, but also actual emission figures, transforming the cooling system into a tool for simultaneously managing efficiency and environmental parameters.

A. Sheikhi *et al.* (2026) formulated thermal management of a heavy-duty six-cylinder diesel engine as a multi-physical problem involving the interaction of combustion, coolant flow and the stress-strain state of components within a coupled Computational Fluid Dynamics – Finite Element Analysis (CFD/FEA) approach. It was demonstrated that local peaks in temperature and stress were determined not only by the flow rate and geometry of the channels, but also by the spatio-temporal distribution of heat release, which made such modelling the basis for flow redistribution and design solutions in critical zones. I. Gritsuk *et al.* (2024) proposed an adapted model for ensuring the thermal readiness of a vehicle, in which fuel flow and emission parameters are considered as integral markers of the engine's thermal state. It has been demonstrated that linking control algorithms to routinely measured operational thermal indicators (in particular, fuel consumption and emission parameters) enables the formulation of rational decisions for warm-up modes and transient processes without the need for highly detailed real-time numerical models.

D.S. Pohorletsky *et al.* (2023) examined the reliability of heat-loaded components in low-speed marine internal combustion engines in relation to low-temperature corrosion, which occurs when specific surface temperature conditions combine with the condensation of aggressive components in the peri-cylinder zone. The study demonstrated that the cooling system acts as a thermochemical regulator: temperature shifts within critical ranges can both minimise the conditions for the condensation of acidic compounds and intensify corrosion processes. The operational aspect of the internal combustion engine cooling system reliability is detailed in terms of the properties of the coolant (antifreeze). In the study by M. Nahliuk *et al.* (2023), a statistically significant correlation was established between antifreeze quality indicators and their electrical conductivity. The possibility of using electrical conductivity as an operational indicator of coolant degradation has been substantiated, which can be used for adjustment of replacement intervals and the reduction of risks of corrosive and electrochemical damage to cooling system components.

Further developments in this applied field are outlined in the work by V.I. Kholdenko (2025), which systematises methods for diagnosing cooling system pumps, with a focus on sensor-based and vibration monitoring. It is shown that the transition to preventive maintenance ensures the stability of coolant flow, maintains the specified heat balance and prevents local overheating. V.V. Pylyov *et al.* (2024) refined the empirical model of the boundary conditions for heat transfer in the piston of a high-speed diesel engine based on experimental data and approximations for identifying temperatures in control zones. It is shown that the reproduction of the mode-dependent temperature field ensures sufficient engineering accuracy in the estimation of thermal stress without increasing computational complexity.

Despite the substantial research devoted to optimisation of pump, water jacket and thermal management strategies, there is a lack of a formalised integrated approach that would simultaneously account for temperature non-uniformity in critical zones, heat dissipation

intensity, fuel efficiency during transient conditions, and the thermomechanical reliability of engine components. In this regard, the study aimed to improve the thermal efficiency and operational reliability of ICEs by developing an integrated methodology for evaluating and optimising the design and control parameters of the cooling system. To achieve this objective, the following tasks were defined: to identify critical zones of ICE and develop a system of quantitative indicators of temperature non-uniformity; to assess the influence of the cooling system configuration and coolant circulation modes on heat dissipation intensity, temperature gradients and the associated stress state of engine components, with the determination of the safety factor; to develop an integrated criterion for optimising the ICE cooling system configuration, incorporating transient warm-up, fuel consumption and thermomechanical reliability indicators.

MATERIALS AND METHODS

The study was conducted between February and October 2025 under laboratory and engine test bench conditions, which enabled the reproduction of steady-state and transient thermal regimes characteristic of the operation of modern petrol internal combustion engines. The subject of the study was a 1.6-litre four-cylinder in-line engine with a closed-loop liquid cooling system and an electronically controlled thermostat. Three cooling system configurations were compared: the standard base system with a mechanical pump (S1), a system with an electric variable-displacement pump (S2), and a configuration with separate cooling circuits for the cylinder block and cylinder head (S3), in which the flow was split after the pump into two parallel branches, "block" and "cylinder head", with the standard internal bypass between the circuits shut off and a fixed flow balance established during bench setup. Comparability of the thermal load between S1-S3 was ensured by identical operating modes in terms of rotational speed and load, as well as by monitoring the effective power at control points following ISO 15550:2016 (2016).

A 50/50 water-glycol solution containing G12++ class corrosion inhibitors was used as the coolant; to improve the accuracy of the heat balance, the density $\rho(T)$ and specific heat capacity $c_p(T)$ were determined experimentally in the range 20-110°C and used as temperature-dependent input data in the heat transfer calculations. Temperatures were monitored using type *K* thermocouples with an error of ±0.5°C in accordance with IEC 60584-1:2013 (2013), and the coolant flow rate was monitored using an electromagnetic flow meter with an accuracy class of no worse than ±1.0%.

Signals were recorded using a multi-channel data acquisition system. Thermal imaging of the external surfaces of the cylinder block and cylinder head (temperature sensitivity 0.04°C) was used as an auxiliary means of detecting areas of local overheating and cooling anomalies; quantitative comparisons were made solely based on thermocouple data at critical control points. Additionally, fuel consumption was recorded at stationary points and during warm-up, followed by calculation of brake-specific fuel consumption (BSFC) and integral fuel consumption until operating temperature was reached. To ensure comparability between S1-S3, all series were conducted under identical external conditions and using the same operating algorithms for the test bench's auxiliary systems; in particular, the air temperature at the radiator inlet and the fan/airflow control mode were kept constant (fixed control signal and stabilisation within the test bench tolerances) to minimise unintended effects on the coolant outlet temperature.

The study was conducted in four interrelated stages. In the first stage, the intensity of heat removal via the cooling system under steady-state conditions was assessed based on measured parameters of the coolant flow. The heat flux through the cooling circuit was calculated using equation (1):

$$\dot{Q}_{cool} = \dot{m} \times c_p \times (T_{out} - T_{in}), \quad (1)$$

where $\dot{Q}_{cool}$ – the heat flux transferred to the coolant circuit (partial heat balance of the cooling circuit); $\dot{m}$ – mass flow rate of the coolant; c_p – specific heat capacity; T_{in} and T_{out} – inlet and outlet temperatures of the engine.

The tests were conducted at speeds of 1,500, 2,500 and 3,500 rpm under loads of 25%, 50% and 75% of the rated load, whilst maintaining the temperature difference ($T_{out} - T_{in}$) within the range of 8-15°C, as is typical for operating conditions. Recording for each "mode-configuration" pair was performed after reaching quasi-steady state, which was determined by the stabilisation of the temperatures T_{in} and T_{out} and the coolant flow rate: for at least 120 s, the change in T_{in} and T_{out} did not exceed 0.2°C/min, and the change in flow rate did not exceed 1% (provided that n and the load remained constant within the bench tolerances). Reproducibility was verified by repeated runs at the reference point of 2,500 rpm and 50% load ($n = 2$) following an identical warm-up and stabilisation protocol, whilst the transient warm-up regime was repeated for each configuration S1-S3 ($n = 2$). The uncertainty of $\dot{Q}_{cool}$ was estimated by propagating the measurement errors $\dot{m}$, T_{in}, T_{out} and the uncertainty $c_p(T)$ following JCGM 100:2008 (2008) approach, and the difference between configurations was interpreted as practically significant if it exceeded the total estimated uncertainty of the corresponding parameters.

In the second stage, a CFD analysis of the flow and heat transfer within the cooling jacket was performed in a coupled "fluid-solid" configuration using ANSYS Fluent 2024 R1 (Ansys, Inc., 2024, USA) based on CAD geometry, solving the Navier-Stokes equations for incompressible turbulent flow using the k-ω SST model and the heat transfer equations (Menter, 1994). For configurations S1-S3, the temperature and velocity fields and local heat transfer coefficients were determined at flow rates of 40, 60 and 80 L/min and T_{in} = 85-95°C. The boundary conditions for T_{in} and flow rate were set within these ranges in accordance with the measured bench test values for each mode; in particular, for the 3,500 rpm and 75% load mode, the CFD analysis was performed for a T_{in}/flow rate combination

corresponding to the bench test parameters of this mode. The computational mesh comprised 3.2-4.5 million elements, and mesh independence was accepted based on a criterion of peak temperature variation <1.5% relative to the base mesh. Validation of the CFD model was performed by comparing the calculated metal temperatures at control points on the cylinder head with experimental readings from *K*-type thermocouples at these same points; the temperatures T_{in} and T_{out} were used as input boundary conditions but were not included in the validation criterion.

Comparisons were conducted for the maximum thermal load condition at 3,500 rpm and 75% load, and additionally for the reference condition at 2,500 rpm and 50% load, which corresponded to the bench test repeatability reference point. In total, six reference points were compared, located in critical zones of the pre-chamber region (valve clearance, exhaust port area) and on the periphery of the cylinder head to assess temperature gradients; a relative deviation between calculation and measurement within 3-5% at each point was considered acceptable. CFD was used as an explanatory tool to interpret the differences between S1-S3, focusing on areas of insufficient flow and local temperature maxima. Due to the lack of replicates for most stationary points, statistical tests were not applied, and comparisons were performed using deterministic metrics, considering the specified measurement instrument errors. The key indicators were T_{max} in critical zones, distributions of heat transfer coefficients, and the identification of areas with insufficient flow as indicators of overheating risk, consistent with experimental temperature trends at control points.

In the third stage, the effect of temperature fields on reliability was assessed via the thermal stress state of the cylinder head in ANSYS Mechanical 2024 R1 (Ansys, Inc., 2024, USA), using the metal temperature fields obtained in the CFD stage in a coupled formulation as boundary conditions. The thermal load from engine operation was applied implicitly via this spatial temperature distribution for the relevant operating modes, without additionally imposing heat fluxes in the strength analysis. The material was modelled as AlSi7Mg, and the parameters $E = 70$ GPa and $\alpha = 22 \times 10^{-6}$ 1/K were specified according to technical tabulated data (Primary Foundry Alloys, n.d.). The calculation was performed in a linearly elastic formulation as a comparative indicator of the influence of cooling configurations without life (cyclic) prediction. Mises equivalent stresses σ_{vM} were calculated, and the safety factor was determined using the accepted reference value $\sigma_{0.2} \approx 240$ MPa, and the threshold $n \geq 1.5$ was applied as an engineering criterion for ranking configurations and localising potentially critical zones.

In the fourth stage, the engine warm-up transient response from 20°C to 90°C was investigated. Warm-up was performed according to a reproducible bench test protocol with a fixed speed of 2,000 rpm and a load of 25% of the rated load (the same for all S1-S3 series) under constant radiator cooling conditions; The initial state was defined as a stabilised coolant temperature of 20 ± 2°C. The time to reach 90°C was determined based on the coolant temperature and control points; additionally, the integral fuel consumption up to 90°C was calculated to establish a quantitative relationship between the cooling strategy and warm-up efficiency. For S2, the electric pump control was varied using a discrete set of at least three performance scenarios depending on the coolant temperature, which were defined as step laws with temperature thresholds and fixed levels of the electric pump control signal (as a percentage of the maximum): (i) "minimum start" – 30% at T < 60°C, 60% at 60-80°C and 100% at T ⩾ 80°C; (ii) "moderate start" – 50% at T < 60°C, 75% at 60-80°C and 100% at T ⩾ 80°C; (iii) "smooth transition" – 40% at T < 50°C, 60% at 50-70°C, 80% at 70-85°C and 100% at T ⩾ 85°C, with switching upon reaching thresholds and a hysteresis of 2°C to prevent frequent switching. For temperature-controlled systems, the effect of thermostat settings was additionally analysed by varying the target opening temperature within the range of 88-92°C and the hysteresis within the range of 3-5°C within the bench-test configuration, and assessing their impact on the heating rate and the amplitude of temperature fluctuations after reaching steady state.

Optimisation involved selecting the best configuration and control settings from among the tested options based on a set of criteria, which simultaneously required a targeted reduction in peak temperature in critical zones by 8-12%, a reduction in temperature gradients by at least 10%, and an improvement in warm-up characteristics (time and/or integral fuel consumption up to 90°C) without compromising power output and without increasing BSFC in the reference steady-state modes relative to S1. The final selection of the "optimal" solution was recorded only when the advantage according to the criteria exceeded the estimated uncertainty of the measurements of heat flux and temperature parameters.

RESULTS

Comparative assessment of heat dissipation under steady-state conditions

An assessment of the heat dissipation rate through the cooling circuit under steady-state conditions in the range of 1,500-3,500 rpm at 25-75% load revealed systematic and reproducible differences between configurations S1-S3, manifested both in the absolute values of the heat flux and in scaling with increasing rotational speed and load. Determination of the heat flux $\dot{Q}_{cool}$ in accordance with formula (1) confirmed a regular increase in heat dissipation intensity with an increase in the engine's thermal load and was used for a quantitative assessment of the impact of design changes to the cooling system. The study established that the upgraded configurations demonstrate a more pronounced response of heat dissipation to increased load compared to the base system. The summarised values of $\dot{Q}_{cool}$, obtained based on the measured parameters of the coolant mass flow rate and the temperature difference at the engine inlet and outlet, are given in Table 1.

Table 1. The value of the cooling heat flux $\dot{Q}_{cool}$ for configurations S1-S3 at speeds of 1,500-3,500 rpm under 25-75% load

n, RPM	Load, %	$\dot{Q}_{cool}$ S1, kW	$\dot{Q}_{cool}$ S2, kW	$\dot{Q}_{cool}$ S3, kW	ΔS2-S1, %	ΔS3-S1, %	U($\dot{Q}_{cool}$), kW
1,500	25	18.0	18.7	19.3	3.9	7.2	±0.5
1,500	50	24.0	25.7	26.4	7.1	10.0	±0.7
1,500	75	31.0	34.1	35.3	10.0	13.9	±0.9
2,500	25	22.0	23.1	23.8	5.0	8.2	±0.7
2,500	50	30.0	32.7	33.6	9.0	12.0	±0.9
2,500	75	40.0	44.8	46.0	12.0	15.0	±1.2
3,500	25	26.0	27.6	28.3	6.2	8.8	±0.8
3,500	50	36.0	40.0	41.0	11.1	13.9	±1.1
3,500	75	48.0	54.2	56.2	12.9	17.1	±1.4

Note: $U(\dot{Q}_{cool})$ is presented as the total estimated standard uncertainty (~3% of the S1 value in the corresponding mode). In all modes, at 50-75% load, the difference between S1 and S2/S3 exceeds the uncertainty limit, confirming the practical significance of the observed differences

Source: compiled by the authors based on JCGM 100:2008 (2008), IEC 60584-1:2013 (2013)

As shown in Table 1, for all configurations, an increase in $\dot{Q}_{cool}$ is observed as the load increases at a fixed rotational speed. Within each mode, an increase in load from 25% to 75% is accompanied by an increase in heat flux of approximately 1.7-2 times (depending on the configuration), which corresponds to an increase in indicated power and total heat release in the cylinders. At the same time, the nature and magnitude of the increase in $\dot{Q}_{cool}$ vary between configurations, indicating differences in heat dissipation efficiency and the cooling system's sensitivity to changes in thermal load. At 75% load during the transition from 1,500 to 3,500 rpm, the increase in $\dot{Q}_{cool}$ was 17 kW for S1, 20.1 kW for S2 and 20.9 kW for S3, reflecting the varying intensity of heat dissipation scaling with increasing steady-state thermal load. At the highest load point of 3,500 rpm and 75% load, S3 demonstrated the greatest deviation from the baseline configuration: the difference relative to S1 was 8.2 kW (17.1%), whilst for S2 it was 6.2 kW (12.9%); in the 50-75% load range, these differences exceeded the total estimated measurement uncertainty, confirming their reproducibility. Analysis of the temperature difference ($T_{out} - T_{in}$) as an indicator of the circuit's thermal load showed that the highest ΔT values were recorded in S1 under high-load conditions (13-15°C), whereas for S2 and S3 under the same conditions, ΔT is lower, by 0.8-1.2°C and 1.5-2.0°C, respectively. A combination of a lower ΔT with an increase in coolant flow rate corresponds to an increase in total heat removal and reflects a change in the heat transfer conditions within the circuit. The minimum difference between S2 and S3 is characteristic of low-load conditions, whereas at high-load points, the dominance of S3 increases, which is consistent with the effect of separating the block and head circuits on targeted cooling supply to areas of increased heat generation compared to a scenario where modernisation is achieved solely through a controlled electric pump. Analysis of repeat measurements at the reference point of 2,500 rpm and 50% load demonstrated reproducibility of results within 2-3%, confirming the stability of the data obtained. The deviations between repeated runs for each configuration did not exceed the total estimated uncertainty; therefore, the average values are representative for comparative analysis.

Overall, the study established that upgrading the cooling system affects not only the absolute values of the heat flux but also the nature of its scaling with increasing load and rotational speed. The S2 configuration ensures a steady increase in $\dot{Q}_{cool}$ across the entire operating range without signs of saturation at high speeds, whereas S3 demonstrates the maximum increase in heat dissipation precisely under conditions of increased thermal load. The difference between S1 and S3 under high-speed and high-load conditions exceeds the estimated measurement uncertainty, rendering it engineering significant.

Temperature distribution and thermal stress state of the cylinder head

The transition from an integrated quantitative assessment of heat dissipation to a spatial analysis of the temperature distribution revealed that the differences between configurations S1-S3 are distinctly local in nature and are caused by the non-uniformity of the flow around individual zones of the cooling jacket. The analysis was performed for the 3,500 rpm mode at 75% load, for which the CFD interpretation was formulated under boundary conditions of T_{in} = 85-95 °C and coolant flow rates of 40/60/80 L/min, which were consistent with the measured bench test parameters corresponding to the maximum $\dot{Q}_{cool}$ values established in steady-state tests. The study determined that it is precisely under increased thermal load that the design features of the cooling systems become most pronounced. A comparison of temperature fields showed that the formation of local maxima is determined by a combination of heat release intensity in the pre-chamber zone and the spatial structure of the coolant velocity field. For the base configuration S1, the highest temperature gradients were found in the inter-valve outlet zone, whereas in S2 and S3, a partial or significant reduction was observed. The identified differences are consistent with the difference in the magnitude of the total heat flux and confirm the systematic influence of the hydrodynamic organisation of the flow on the thermal state of critical components. To interpret the causes of the identified differences between the configurations, a CFD analysis of the temperature fields in the cooling jacket was performed (Fig. 1).

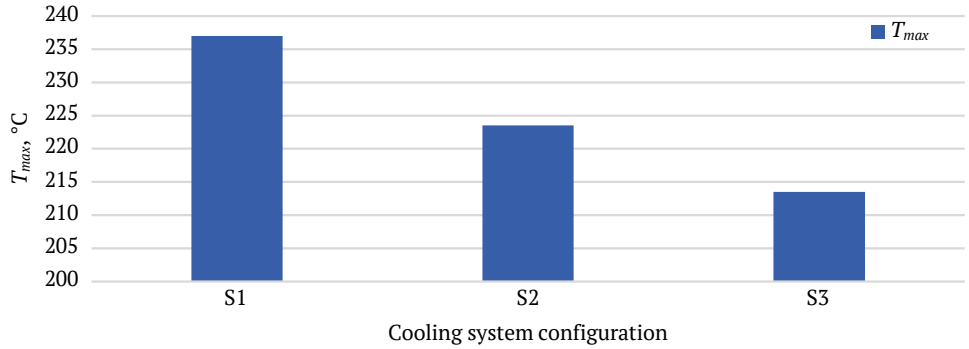

Figure 1. T_{max} in the critical area of the cylinder head for configurations S1-S3
Note: sidebars on the columns indicate the minimum and maximum T_{max} values recorded within the relevant series of calculations
Source: compiled by the authors based on F.R. Menter (1994), IEC 60584-1:2013 (2013)

Following Figure 1, in configuration S1, a local temperature maximum forms in the area between the exhaust valves of the first and second cylinders. The peak temperature T_{max} in this region was 236-238°C, which is 18-22°C higher than the average temperature across the cylinder head. Spatial analysis revealed a region of reduced coolant velocity in this zone, accompanied by a local decrease in the heat transfer coefficient and the formation of a superheated region. In the S2 configuration, the maximum temperature in the corresponding zone decreased to 222-225°C, corresponding to a reduction of 5-6% compared to S1. Comparison with the steady-state heat balance showed that the increase in coolant flow rate ensured intensified heat removal from the pre-chamber region. At the same time, the temperature distribution remained partially non-uniform: local peaks persisted near the walls of the water jacket, indicating that the hydrodynamic restrictions had not been fully eliminated. The most uniform temperature distribution was recorded in the S3 configuration. T_{max} in the critical zone did not exceed 212-215°C, corresponding to a reduction of approximately 9-11% compared to S1. At the same time, the internal temperature gradients between the pre-chamber and peripheral zones within a single cylinder decreased from 28-30°C for S1 to 18-20°C for S3, i.e. by approximately 30-35%. The separation of the cooling circuits ensured that most of the coolant flow was directed towards areas of intense heat generation and minimised parasitic flow, which stabilised temperature distribution and reduced localised peak loads.

Analysis of heat transfer coefficient h fields showed that in S1, the minimum values were localised at the rear of the cylinder head and in the area where the jacket channels converge, where h fell to 2,400-2,600 W/(m²·K), which is 18-20% lower than the average value across the surface. In S2, the minimum values increased to 2,700-2,900 W/(m²·K), whilst the area of their localisation decreased. For S3, an increase in the minimum local values to 3,100-3,300 W/(m²·K) was observed, along with the virtual absence of stagnant zones in the pre-chamber region. A comparison of the velocity fields confirmed that in S1, regions with reduced turbulent intensity formed, which limited convective heat transfer. In S2, the intensification of circulation increased local velocities, although geometrically induced recirculation zones were partially retained. In S3, the redistribution of flows smoothed the velocity profile and increased the average heat transfer coefficient in the zone of maximum thermal load by 12-15% compared to S1.

A comparison of the CFD results with experimental data from control points demonstrated a high degree of agreement: the calculated temperatures differed from the measured values by no more than 3-4%. The location of T_{max} coincided with the points of elevated temperature recorded by thermocouples in the exhaust port area, confirming the adequacy of the model. Analysis of temperature gradients within the cylinder head revealed that in S1, the difference between the maximum and minimum temperatures within a single cylinder reached 28-30°C. In S2, this figure decreased to 22-24°C, and in S3, to 18-20°C. The study established that the reduction in internal temperature gradients is directly linked to an increase in heat transfer uniformity. Thus, the CFD analysis showed that differences in total heat dissipation have a clear spatial basis. In S1, localised areas of insufficient flow cause the formation of peak temperatures and elevated gradients. In S2, intensified circulation reduces T_{max} but does not eliminate hydrodynamic limitations. In S3, the separation of the circuits ensures the most uniform temperature distribution and an increase in local heat transfer coefficients. The decrease in T_{max} in this configuration is consistent with the increase in $\dot{Q}_{cool}$ and is accompanied by a reduction in temperature gradients, which forms the basis for a further assessment of the thermal stress state.

The analysis of the thermal stress state revealed that the spatial distribution of equivalent stresses according to von Mises showed a clear correlation between the location of temperature maxima and the magnitude of temperature gradients in the near-chamber zones. The study established that the determining factor in the formation of local thermal stresses is precisely the amplitude of the temperature gradients, whilst the absolute level of the average temperature has a secondary influence. A comparison of

the temperature and stress fields confirmed the coincidence of σ_{vM} concentration zones with areas of increased thermal heterogeneity, which attests to a cause-and-effect relationship between the nature of heat transfer and the stress state of the structural element. The results obtained showed that the non-uniformity of the temperature field determines the intensity of the thermomechanical load in critical zones of the cylinder head, primarily in the inter-valve space and in the area of the exhaust valve seats. To quantitatively illustrate the influence of temperature fields on the stress state, the distribution of equivalent stresses σ_{vM} is shown in Figure 2.

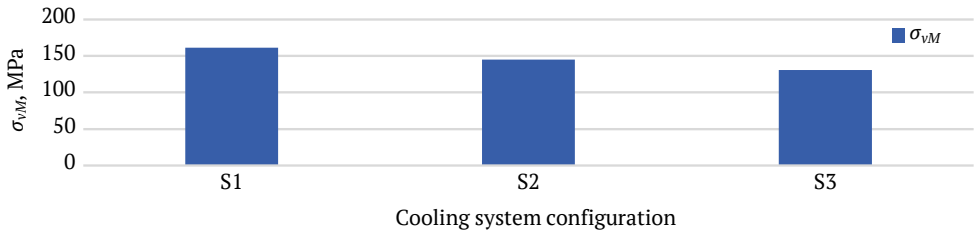

Figure 2. Maximum equivalent stresses σ_{vM} in the critical zones of the cylinder head for configurations S1-S3
Note: calculated for an operating speed of 3,500 rpm and a load of 75%. The bars represent the average values of the maximum equivalent stresses σ_{vM} in the critical zones; side-bars represent the min-max range corresponding to the minimum and maximum values of σ_{vM} recorded in the respective series
Source: compiled by the authors based on F.R. Menter (1994), Primary Foundry Alloys (n.d.)

As shown in Figure 2, in the base configuration S1, the maximum equivalent stresses were concentrated in the area between the exhaust valve seats of the first and second cylinders, as well as in the bridges between the combustion chambers. At 3,500 rpm under 75% load, the σ_{vM} values reached 158-165 MPa (average 161.5 MPa), and spatial comparison confirmed that these regions coincided with the zones of elevated temperature gradients identified in the previous stage, indicating that the formation of the stress state was thermally induced. In the S2 configuration, the maximum values of σ_{vM} decreased to 142-148 MPa (average 145.0 MPa), corresponding to a reduction of 8-10% compared to S1; at the same time, the levelling of the temperature field and the decrease in T_{max} were accompanied by a reduction in the amplitude of local deformations. The nature of stress localisation in S2 generally remained in the pre-chamber region, but the area of the high-stress zone decreased by approximately 12-15%, indicating a reduction in the degree of localisation of the thermally stressed state. The lowest values of σ_{vM} were found for the S3 configuration: in the critical zones, they did not exceed 128-134 MPa (average 131.0 MPa), which is 18-22% lower than for S1; the stress distribution became more uniform, and the peak values lost the form of sharply pronounced local concentrations. Thus, the separation of the cooling circuits ensured not only a reduction in T_{max}, but also a quantitatively confirmed decrease in equivalent stresses in the cylinder head.

The structural reliability assessment showed that for S1, under maximum thermal load conditions, the safety factor decreased to $n = 1.45\text{-}1.52$, whilst in certain sections of the crossbeams it approached the threshold value of $n \geqslant 1.5$, indicating that these areas are particularly sensitive to thermal cycling. In S2, the safety factor increased to 1.62-1.69 in the most heavily loaded sections, ensuring consistent compliance with the criterion throughout the entire volume of the cylinder head. The most favourable indicators were observed in S3: n ranged from 1.78 to 1.87 in critical zones and exceeded the threshold value by a significant margin in all investigated conditions. Analysis of the stress distribution across the thickness of the block head confirmed that in S1, temperature gradients created a combination of tensile stresses in the near-surface layers and compressive stresses deeper within the material; the difference between them exceeded 60 MPa. In S2, this difference decreased to 45-50 MPa, and in S3 to 35-40 MPa, which is consistent with the levelling of the temperature field and the reduction of internal thermomechanical gradients. Thus, the results of the thermal stress analysis confirmed a clear cause-and-effect relationship between the cooling system architecture, the nature of the temperature field, and the level of thermal stresses in the cylinder head. The reduction in T_{max} and temperature gradients in the S3 configuration was accompanied by a significant decrease in σ_{vM} and an increase in the safety factor, confirming its superiority in terms of durability and thermal reliability compared to S1 and S2.

Analysis of the transient warm-up regime

An analysis of the transient warm-up behaviour, conducted under reproducible bench test conditions with an initial coolant temperature of 20 ± 2°C, revealed significant differences in the dynamics of the engine reaching its operating temperature for configurations S1-S3. The time taken to reach operating temperature was determined by the average coolant temperature in the main circuit reaching 90°C. The study established that the cooling system architecture directly influences the duration of the transient process and the intensity of the initial heating, which is reflected both in the time taken to reach 90°C and in the nature of the temperature curve. The dynamics of engine warm-up from 20 to 90°C for configurations S1-S3 are shown in Figure 3.

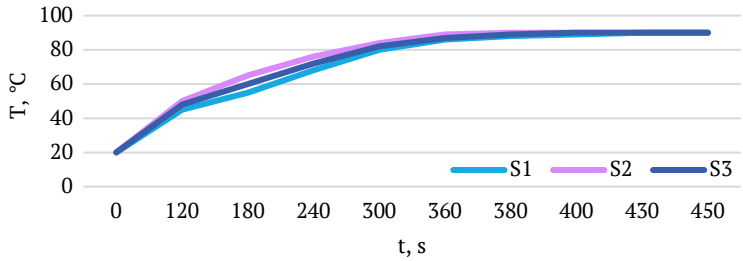

Figure 3. Coolant temperature curves for configurations S1-S3
Source: compiled by the authors based on JCGM 100:2008 (2008), IEC 60584-1:2013 (2013)

The data shown in Figure 3 demonstrates that the use of a variable-capacity electric pump resulted in a faster reach of the operating temperature range compared to the baseline configuration. For S1, the time taken to reach 90°C averaged 420-435 s, whereas for S2 this figure fell to 370-385 s, representing a reduction of 9-12%. Configuration S3 demonstrated an intermediate result – 395-405 s, corresponding to a 6-8% reduction in warm-up time relative to S1. The reduction in warm-up time achieved in S2 and S3 exceeds the limits of the total estimated measurement uncertainty, confirming the engineering significance of the effect. Analysis of the temperature curves showed that in S1, the heating process is nearly linear until the thermostat opens, after which the rate of temperature rise decreases due to the connection of the main circuit and the activation of circulation through the radiator. In the S2 configuration, a more intense initial rise in temperature was observed, which correlates with a reduction in the electric pump's performance during the cold start phase. The restriction of coolant flow in the first few minutes of operation was accompanied by a reduction in heat dissipation and an acceleration in reaching the operating temperature range without exceeding permissible values. For S3, the warm-up behaviour remained stable and controlled: the initial phase was more intense than in S1, but less pronounced compared to S2, reflecting the effect of circuit separation under constant circulation parameters.

The total fuel consumption up to 90°C showed a clear correlation with the duration of the warm-up. For S1, this figure was 0.082-0.086 kg of fuel, whilst for S2 it decreased to 0.073-0.076 kg, corresponding to a saving of 10-12%. In the S3 configuration, the integral consumption was 0.078-0.080 kg, i.e., a reduction of 5-7% compared to the base system. The comparison showed that the fuel savings achieved exceed the limits of experimental uncertainty and are statistically significant.

It has been established that reducing the duration of engine operation in the rich-mixture mode directly reduces the total fuel consumption during the transition phase. Further analysis of electric pump control scenarios in S2 showed that using a minimum flow rate until 60°C is reached, followed by a stepwise increase in coolant flow, resulted in the shortest warm-up time – approximately 370 s. When a smooth linear dependence of flow rate on temperature was applied, the warm-up time increased by 4-6%, but the amplitude of temperature fluctuations after the thermostat opened decreased. The comparison confirmed that a discrete strategy with clearly defined temperature thresholds provides better fuel efficiency without adversely affecting thermal stability. Analysis of steady-state conditions after warm-up completion revealed no increase in BSFC for S2 and S3 relative to S1. At 2,500 rpm under 50% load, the difference in BSFC between S1 and S2 did not exceed 1.5%, which is within the experimental uncertainty. Thus, accelerated warm-up is not accompanied by a deterioration in fuel efficiency under steady-state conditions.

Temperature fluctuations after reaching 90°C were considered as an indicator of the stability of thermal regulation. In S1, the amplitude of the fluctuations was 6-8°C, whereas in S2, under the optimal control algorithm, it decreased to 4-5°C. In S3, the amplitude was 5-6°C. It was established that adaptive control of coolant flow rate contributes to increased thermal stability after reaching operating temperature. Thus, the results of the transient analysis showed that configuration S2 provides the shortest warm-up time and minimum integral fuel consumption without compromising BSFC performance in steady-state conditions. Configuration S3 demonstrates a moderate reduction in warm-up time and fuel consumption, whilst simultaneously improving temperature uniformity and reducing the thermal stresses identified previously. The data obtained confirmed that optimising the cooling system can simultaneously improve the engine's thermal reliability and fuel efficiency, and that adaptive control of the electric pump's performance is an effective tool for reducing fuel consumption in cold start conditions without adversely affecting steady-state operating characteristics.

Integral ranking and selection of the optimal configuration

A comprehensive analysis of the results from all stages of the study has shown that the differences between configurations S1-S3 are systematic in nature and manifest simultaneously in terms of heat dissipation, temperature uniformity, thermal stress, and fuel efficiency during transient operation. The generalisation was conducted by directly comparing quantitative indicators with the accepted optimisation criteria without introducing additional empirical coefficients or new input data. For a comprehensive

assessment of the efficiency of the configurations under study, a generalised matrix of optimisation criteria was formed, in which, for each variant S1-S3, the achieved level of reduction in peak temperatures, internal temperature gradients, equivalent stresses, as well as indicators of transient and steady-state fuel efficiency are shown (Table 2).

Table 2. Comparative matrix of optimisation criteria for S1-S3

Criteria	S1	S2	S3
Reduction in T_{max} relative to S1	-	5-6%	10-12%
Reduction in temperature gradients	-	18-22%	30-35%
Maximum σ_{vM}, MPa	158-165	142-148	128-134
Safety factor n	1.45-1.52	1.62-1.69	1.78-1.87
Reduced warm-up time	-	9-12%	6-8%
Reduction in overall fuel consumption	-	10-12%	5-7%
Changes in BSFC under steady-state conditions	-	⩽1.5%	⩽1.5%
Excess of the effect over the estimated measurement uncertainty ($\dot{Q}_{cool}$, T_{max}, ΔT)	-	confirmed	confirmed

Source: compiled by the authors based on F.R. Menter (1994), JCGM 100:2008 (2008)

Analysis of the data in Table 2 showed that the base configuration S1, under maximum thermal load conditions, is characterised by peak temperatures and stresses that locally approach the threshold conditions for long-term reliability. The safety factor n for S1 decreased to 1.45-1.52, i.e., in certain inter-valve zones it reached the minimum permissible level of 1.5. A comparison with the results of the spatial temperature analysis confirmed that the key cause of critical stresses is precisely temperature inhomogeneity and high internal gradients, rather than merely the absolute level of the metal's average temperature. Regarding the criterion of reducing T_{max} by 8-12%, it was found that configuration S2 reduced the peak temperature in critical zones by only 5-6%, i.e., it did not reach the specified range, although it demonstrated a noticeable improvement compared to S1. In contrast, configuration S3 demonstrated a reduction in T_{max} of 10-12%, which fully meets the specified limit and ensures a significant "reduction" in peak temperatures from potentially dangerous levels. This indicates that it is the structural modernisation of the cooling system (separation of the block and head circuits) that has a decisive influence on maximum temperatures in the areas of greatest thermal load. Concerning the criterion of reducing temperature gradients by at least 10%, it was found that the S2 configuration reduced internal temperature gradients by approximately 18-22% compared to S1; that is, the result exceeded the minimum acceptable level and indicates a noticeable smoothing of the difference between the near-surface and deeper layers. In configuration S3, an even more significant reduction in temperature gradients of 30-35% was recorded, indicating a qualitatively different degree of thermal field equalisation. The consistency of this effect with the results of the CFD analysis confirmed that the separation of the cooling circuits provides a structural, rather than a local compensatory, reduction in thermal heterogeneity, which is of fundamental importance for the durability of the cylinder head.

An assessment of the thermal stress state showed that the maximum values of σ_{vM} decreased from 158-165 MPa in S1 to 142-148 MPa in S2 and to 128-134 MPa in S3; that is, the total reduction for S3 was approximately 18-22% compared with the base configuration. This was directly reflected in an increase in the safety factor to 1.78-1.87 in S3. The study established that for this configuration, the criterion $n \geqslant 1.5$ was met with a significant margin in all modes considered, whereas in S2 the value $n = 1.62$-1.69 ensured reliable compliance with the threshold, but with a narrower "safety margin". Thus, in terms of long-term strength and resistance to thermal cycling loads, S3 has the most favourable margin, whilst S2 remains a compromise between improved warm-up and reduced stresses. Transient analysis showed that the shortest warm-up time was achieved by the S2 configuration: the reduction was 9-12% compared to S1, with a corresponding decrease in total fuel consumption of 10-12%. For S3, the warm-up time was reduced by 6-8%, and the integral fuel consumption by 5-7%, which also exceeds the limits of experimental uncertainty. The comparison confirmed that the effects of both upgraded configurations in transient mode are engineering-significant and provide real fuel savings in cold start mode. However, the analysis of steady-state conditions revealed no deterioration in BSFC for S2 and S3: the differences did not exceed 1.5% and fell within the experimental margin of error, determining a trade-off of the "faster warm-up – poorer efficiency" type at the reference steady-state points.

A comprehensive comparison based on uncertainty analysis showed that, for the key criteria – reduction of T_{max}, reduction of σ_{vM} and reduction of warm-up time – the advantage of S2 and S3 over S1 exceeds the limits of the total measurement uncertainty by a factor of 2-3, confirming the reliability and practical significance of the established differences. At the same time, the integrated ranking revealed different "specialisations" of the upgrades: configuration S2 demonstrated the greatest effect in terms of transient thermal and fuel efficiency, whilst S3 provided the best balance between reducing peak temperatures, minimising temperature gradients and increasing the safety factor without any deterioration in steady-state fuel economy. Thus, the results of the integrated ranking showed that the S3 configuration is the most balanced engineering-determined

solution among the options studied, as it is the only one that fully meets the criteria for reducing T_{max} (8-12%) and decreasing temperature gradients (by at least 10%, with an actual reduction of 30-35%) whilst providing an increased safety margin ($n \geqslant 1.5$ with a substantial reserve) and no deterioration in BSFC under steady-state conditions. The comparison confirmed that the advantages of S3 are quantitatively proven and exceed the total measurement uncertainty, which justifies recommending this particular configuration as optimal in terms of improving thermal efficiency, durability and engine reliability.

DISCUSSION

The results of thermal modelling and experimental measurements showed that the architecture of the cooling system determined not only the overall level of heat dissipation, but also the spatial structure of the temperature field and the associated thermal stress state of the cylinder head. The increase in $\dot{Q}_{cool}$ in configurations S2 and S3, the reduction in T_{max} in critical inter-valve zones to 222-225°C and 212-215°C, respectively, as well as the reduction in internal temperature gradients to 18-20°C for S3 is consistent with the concept of nodal thermal modelling proposed by D. Chalet *et al.* (2017), according to which local overheating of cylinder head components arises due to the uneven distribution of heat fluxes between functional nodes and the restriction of convective heat transfer in individual channels. The study demonstrated that optimising coolant circulation trajectories and redistributing flows between subsystems makes it possible to simultaneously reduce peak temperatures and equalise the thermal field. This mechanism was replicated for S3, where the separation of the block and head circuits ensured an increase in the minimum local heat transfer coefficients and a reduction in stagnant flow zones. The identified relationship between the magnitude of temperature gradients and the level of equivalent stresses σ_{vM} confirmed the decisive role of spatial heterogeneity in heating, rather than just the absolute temperature of the metal.

The CFD results for S3 demonstrated an increase in the minimum local heat transfer coefficients and the virtual elimination of stagnation and recirculation zones in the pre-chamber region, indicating a change in the coolant flow path as the mechanism for reducing temperature peaks. This interpretation is consistent with the findings of L. Tan *et al.* (2023), who attributed the reduction in local overheating to the shortening of inefficient hydrodynamic paths and the redistribution of flow between branches. In terms of the causal chain, the effect was described as "modification of channel geometry → smoothing of the velocity profile → increase in local h → reduction in temperature gradients", which explained the simultaneous reduction in T_{max} and smoothing of the temperature profile in S3. Furthermore, H. Salehi *et al.* (2023) demonstrated experimentally and numerically that passive flow control in cooling channels reduces the proportion of recirculation zones, increases the intensity of local convection, and lowers peak metal temperatures. The S3 data obtained in the present study reproduced this mechanism and indicated the priority of structural improvement of the circulation path over simply increasing the flow rate. Therefore, the CFD/FEA structural block is consistent with the coupled heat transfer approach and can be reduced to a single mechanism: reorganising the flow in the cooling jacket increases the local h and eliminates stagnation and recirculation zones, which reduces T_{max}, stabilises the temperature field (reducing gradients), and, as a result, reduces σ_{vM} whilst increasing the safety margin. A. Pandey *et al.* (2024) demonstrated that "hot spots" were caused by the combined effect of convection within the channels, thermal conductivity in the metal and adjacent circuits; consequently, hydrodynamic changes were systematically translated into the stress state. Following the same line of reasoning, L. Yang *et al.* (2024) established those geometric modifications which smooth the velocity field and eliminate recirculation and stagnation reduce local overheating, corresponding to the S3 configuration with a sustained reduction in peak temperatures, temperature gradients and σ_{vM} in the context of an increase in $\dot{Q}_{cool}$.

Transient warm-up analysis showed that S2 reduced the time taken to reach 90°C by 9-12% and lowered the total fuel consumption by 10-12%. Similarly to R. Bakatwar *et al.* (2018), limiting coolant flow at start-up reduces heat loss during the "cold" phase and accelerates entry into the operating temperature window. The temperature-threshold strategy for controlling the electric pump was interpreted within this same causal framework: reducing output to 60°C ensured heat accumulation in the early phase without exceeding permissible limits. Once the thermostat opened, the key factor was not so much the absolute temperature as the stability of the operating mode, and the reduction in the amplitude of fluctuations to 4-5°C in S2 was consistent with the findings of H. Savaripour *et al.* (2022) for a thermostat with map-based control, where temperature-dependent flow control reduced overshoot during the transition to steady-state conditions. A pattern emerged: adaptive control simultaneously reduced warm-up time and stabilised the temperature field without compromising steady-state fuel efficiency (BSFC did not rise beyond the uncertainty limit), whereas integral ranking revealed different "specialisations" of the upgrades: S2 maximised the gain in the transient phase, whilst S3 ensured a deeper structural reduction in T_{max} and gradients with a direct transition to a less thermally stressed state. The trends obtained supported the interpretation of the cooling system as a controlled loop in transient modes. S.-J. Jeong *et al.* (2024) demonstrated that the switching speed of the controlled elements and the flow control algorithm altered the shape of the temperature curve; consequently, the control system itself determined both the heating rate and the amplitude of oscillations once steady-state conditions were reached.

Following the same logic, the results of S2 correlated with the predictive control approach proposed by A. Kaleli (2020),

where the predictive adjustment of the coolant flow rate accelerated warm-up and suppressed oscillations through a feedforward action; in the case under consideration, this principle was implemented through a threshold restriction on circulation in the early phase, followed by a controlled increase. In contrast, the advantage of S3 under heavy loads is consistent with the load- and speed-sensitive cooling map approach proposed by A. Naderi *et al.* (2021). In their study, optimal thermal behaviour was achieved not by a constant increase in flow rate, but by its targeted adaptation to the thermal load. In the presented study, the separation of circuits in S3 ensured that cooling resources were prioritised for areas of maximum heat dissipation; consequently, the effect naturally intensified with increasing load and manifested as a more significant reduction in T_{max} and temperature gradients than in S2.

The accelerated warm-up and temperature stabilisation were not accompanied by a deterioration in BSFC at steady-state points (differences ⩽1.5% within the margin of uncertainty). B. Lu *et al.* (2023) emphasised the need to maintain a stable temperature "window" under non-design conditions to prevent efficiency losses during integration with waste heat recovery circuits. In this context, the reduction in the amplitude of temperature fluctuations in configurations S2 and S3 after reaching the operating level was interpreted as the establishment of a controlled temperature regime, compatible with the subsequent expansion of energy integration. Such stabilisation of the temperature profile after reaching the operating level was consistent with approaches to predictive model control in vehicle thermal management tasks, where the regulation of coolant flow was considered as a tool for simultaneously minimising heat losses during the warm-up phase and adhering to constraints regarding temperature stability and the risk of local overheating in transition zones. In the study by P. Lu *et al.* (2019), Model Predictive Control (MPC) was described as an approach to coordinating heat transfer between the under-bonnet space and thermal subsystems, within which flow control performed an energy-oriented function without losing stabilisation capability. In this causal framework, the S2 effect was interpreted as a controlled change in the effective "thermal resistance" during the warm-up phase (restriction of circulation followed by a controlled increase), whilst the reduction in oscillation amplitude after reaching the operating temperature reflected the absence of overshoot and compliance with temperature limits.

The results regarding temperature stabilisation after reaching steady state correlated with approaches involving integrated valve modules and multi-channel flow control. L. Pimpinella *et al.* (2021) demonstrated that such modules provided more accurate flow distribution between branches, improving the stability of the cooler temperature and reducing overshoot. In the case under consideration, a similar effect was achieved through the electric pump control algorithm and the split-loop architecture, i.e., through controlled flow redistribution, which reduced thermal mode fluctuations. This is consistent with the review by H. Liu *et al.* (2021), which highlighted the shift from passive temperature maintenance to active thermal management using controlled pumps, thermostats and mode-dependent maps. Within this framework, the results obtained demonstrated the functional differentiation of the upgrades: S2 provides the best warm-up performance and fuel economy in cold mode, whilst S3 produces a more uniform temperature field and minimal thermal stresses, which explains its advantage in terms of durability. Further development of this approach was linked to hybrid "simulation + machine learning" solutions. Y. Zou *et al.* (2025) demonstrated the possibility of predicting the performance of electric fans and electric pumps based on a combination of modelling and machine learning, which created the possibility of more precise control under variable operating conditions. In the context of the results obtained, this is relevant as the performance of S2 in cold mode remained sensitive to the parameterisation of the control algorithm, and improving the accuracy of the prediction made it possible to maintain the fuel efficiency whilst ensuring temperature stability.

From an energy efficiency perspective, the findings are consistent with the approach of minimising the parasitic power of the cooling system. P.H.A. Brayner *et al.* (2024) demonstrated that reducing the power consumption of the pump or fan drive can improve fuel economy without compromising the engine's thermal performance. The observed fuel savings in transient mode for S2 were explained precisely by this mechanism: a reduction in the electric pump's output during a cold start reduced the energy costs of circulation and limited heat dissipation, thereby shortening the duration of the cold phase. At the same time, the absence of noticeable changes in BSFC at steady-state points confirmed that the effect of minimising parasitic power was primarily evident in dynamic modes.

This interpretation was supported by models of bypass circulation circuits. R.I.A. Jalal *et al.* (2021) demonstrated that a bypass electric water pump reduced warm-up time by limiting heat dissipation in the "large" circuit during the early stages and concentrating heat to accelerate warm-up. Although in S2 this effect was achieved through variable capacity, the underlying mechanism remained similar – controlled circulation restriction reduced heat loss and shortened the duration of the cold phase. In this same context, G. Kaltakkıran (2021) emphasised that during warm-up, the cooling strategy determined the distribution of energy between useful work, metal heating and losses to the environment. The practical significance of this effect is also confirmed by the results of M. di Bartolomeo *et al.* (2023), which show that the electric pump delivered measurable fuel savings and CO_2 reductions provided that control was coordinated with the engine's thermal requirements across the various phases of the cycle. The bench test results demonstrated a similar pattern: savings were achieved by shortening the cold phase, whilst a stable temperature window was maintained at steady-state points without any

deterioration in BSFC. To extend the observed effects to a wider operating range, a coordinated description of heat transfer and hydraulic losses is required, as these components determine the limits of further parametric optimisation. The study by A. Jafari *et al.* (2022) demonstrates that the error in predicting the performance of a cooling system is determined by the degree of consistency between the heat transfer and pressure loss models, which influence temperature stability and the energy consumption of the circulation. In this context, the results obtained were interpreted as a consequence of the control and architecture under fixed radiator characteristics and hydraulic resistances, which imposed constraints on the subsequent tuning of parameters and determined the conditions for reproducibility across a wider range of operating modes.

An analysis of the experimental data and numerical simulations showed that combining structural optimisation of the cooling circuit with adaptive flow control created a unified circuit of thermo-hydrodynamic and thermomechanical processes, within which T_{max}, internal temperature gradients and σ_{vM} were reduced, whilst the safety margin increased, whilst fuel savings during warm-up were achieved without compromising BSFC at steady-state points. This reflected the integration of duct geometry, mode-dependent control and energy coordination within a single engineering loop of the engine cooling system's operation.

CONCLUSIONS

This study conducted a comprehensive assessment of the impact of the cooling system architecture on the thermal efficiency, thermal stress conditions and fuel economy of a petrol internal combustion engine under steady-state and transient conditions. The study demonstrated that the modernisation of the standard S1 system using a variable-capacity electric pump (S2) and the separation of the block and head cooling circuits (S3) results in systemic differences that manifest themselves consistently in terms of heat dissipation, temperature fields, stresses and warm-up dynamics. In steady-state conditions, an increase in the heat flux $\dot{Q}_{cool}$ for S2 and S3 of 10-17% relative to S1 has been established in zones of maximum thermal load, accompanied by a reduction in ΔT between the inlet and outlet under constant external conditions, i.e., an intensification of convective heat transfer without circuit overload.

CFD analysis confirmed that the reduction in peak temperatures in the pre-chamber zones is 5-6% for S2 and 10-12% for S3, whilst internal temperature gradients decrease by approximately 18-22% and 30-35% respectively, reflecting a transition from localised overheated regions in S1 to a more uniform temperature field in S3. This correlates directly with a decrease in equivalent stresses σ_{vM} from 158-165 to 128-134 MPa and an increase in the safety factor n from 1.45-1.52 to 1.78-1.87, meaning that in the S3 configuration, the criterion $n \geqslant 1.5$ is met with a significant margin for all analysed modes. In the transient warm-up mode, it was found that the S2 variant reduces the time to reach 90°C by 9-12% and decreases the integral fuel consumption by 10-12% compared to S1, whilst S3 provides a moderate, but reproducible reduction in these indicators of 6-8% and 5-7% respectively, whilst simultaneously improving temperature uniformity. Analysis of BSFC in control steady-state modes showed that accelerated warm-up and modernisation of the cooling system are not accompanied by a statistically significant deterioration in fuel efficiency: the differences do not exceed the limits of experimental uncertainty. Integral ranking accounting for uncertainty confirmed that the S2 configuration is the most effective in terms of minimising warm-up time and fuel consumption in cold-start mode, whereas configuration S3 provides the best balance between reducing T_{max}, minimising temperature gradients, reducing σ_{vM} and establishing an increased safety margin without compromising fuel efficiency.

The results obtained provide a sound basis for recommending S3 as the optimal engineering solution for improving the thermal reliability and durability of internal combustion engines, whilst S2 should be considered a targeted option for applications where reducing warm-up time and emissions during the cold start phase is a priority. Further research should analyse long-term cyclic operation of the upgraded systems, adapting the pump control algorithms to different load profiles, and scaling the proposed solutions to other engine types and displacement volumes.

ACKNOWLEDGEMENTS

None.

FUNDING

None.

CONFLICT OF INTEREST

None.

REFERENES

[1] Bakatwar, R., Nesamani, K., Bhargava, A., & Jain, R. (2018). Performance analysis & optimization of engine cooling system by using electronically controlled thermostat for improving thermal efficiency. *SAE Technical Paper*. doi: 10.4271/2018-01-0053.

[2] Brayner, P.H.A., da Costa, J.Â.P., Ochoa, A.A.V., Urbano, J.J., Leite, G.N.P., & Michima, P.S.A. (2024). Analysis and optimization of the fuel consumption of an internal combustion vehicle by minimizing the parasitic power in the cooling system. *Processes*, 12(2), article number 321. doi: 10.3390/pr12020321.

[3] Chalet, D., Lesage, M., Cormerais, M., & Marimbordes, T. (2017). Nodal modelling for advanced thermal-management of internal combustion engine. *Applied Energy,* 190, 99-113. doi: 10.1016/j.apenergy.2016.12.104.

[4] Di Bartolomeo, M., Di Battista, D., & Cipollone, R. (2023). Experimentally based methodology to evaluate fuel saving and CO_2 reduction of electrical engine cooling pump during real driving. *SAE International Journal of Engines,* 16(5), 693-708. doi: 10.4271/03-16-05-0041.

[5] Di Battista, D., di Bartolomeo, M., & Cipollone, R. (2026). The performance of engine coolant control strategies on real driving emissions. *Applied Thermal Engineering*, 289(1), article number 129753. doi: 10.1016/j.applthermaleng.2026.129753.

[6] Gritsuk, I., Pohorletskyi, D., Bulgakov, M., Khudiakov, I., Volodarets, M., Smyrnov, O., Korohodskyi, V., Symonenko, R., Holovashchenko, O., & Hrytsuk, V. (2024). Development of an approach to the construction of an adapted model for ensuring the thermal readiness processes of a vehicle based on fuel consumption and exhaust gas emissions. *Eastern-European Journal of Enterprise Technologies*, 6(4(132)), 26-45. doi: 10.15587/1729-4061.2024.316922.

[7] IEC 60584-1:2013. (2013). *Thermocouples – part 1: EMF specifications and tolerances*. Retrieved from https://webstore.iec.ch/en/publication/2521.

[8] ISO 15550:2016. (2016). *Internal combustion engines – determination and method for the measurement of engine power – general requirements*. Retrieved from https://www.iso.org/standard/70030.html.

[9] Jafari, A., Sadeghianjahromi, A., & Wang, C.-C. (2022). Experimental and numerical investigation of brazed plate heat exchangers – a new approach. *Applied Thermal Engineering,* 200, article number 117694. doi: 10.1016/j.applthermaleng.2021.117694.

[10] Jalal, R.I.A., Yusoff, M.A.M., Hasan, H.M.A., & Yahya, M.N. (2021). Simulation of bypass electric water pump to reduce the engine warm-up time. *Journal of Mechanical Engineering Science,* 15(3), 8241-8252. doi: 10.15282/jmes.15.3.2021.03.0647.

[11] JCGM 100:2008. (2008). *Evaluation of measurement data – guide to the expression of uncertainty in measurement.* Retrieved from https://www.bipm.org/documents/20126/2071204/JCGM_100_2008_E.pdf.

[12] Jeong, S.-J., Kang, J.-H., Moon, S.-J., & Lee, G.-S. (2024). Transient and dynamic simulation of the fluid flow through five-way electric coolant control valve of a 100 kW fuel cell vehicle by CFD with moving grid technique. *Actuators*, 13(3), article number 110. doi: 10.3390/act13030110.

[13] Kaleli, A. (2020). Development of the predictive based control of an autonomous engine cooling system for variable engine operating conditions in SI engines: Design, modeling and real-time application. *Control Engineering Practice,* 100, article number 104424. doi: 10.1016/j.conengprac.2020.104424.

[14] Kaltakkıran, G. (2021). A study on the effects of coolant strategy on the instantaneous energy balance during the warm-up period in a spark ignition engine. *International Journal of Innovative Research and Reviews,* 5(2), 1-8.

[15] Kholdenko, V.I. (2025). Analysis of existing methods for diagnostic of ship pumps. *Visnyk of Kherson National Technical University*, 1(2(93)), 280-286. doi: 10.35546/kntu2078-4481.2025.2.1.36.

[16] Li, W., Li, E., Shi, W., Li, W., & Xu, X. (2020). Numerical simulation of cavitation performance in engine cooling water pump based on a corrected cavitation model. *Processes,* 8(3), article number 278. doi: 10.3390/pr8030278.

[17] Liu, H., Wen, M., Yang, H., Yue, Z., & Yao, M. (2021). A review of thermal management system and control strategy for automotive engines. *Journal of Energy Engineering,* 147(2). doi: 10.1061/(ASCE)EY.1943-7897.0000743.

[18] Lu, B., Zhang, Z., Cai, J., Wang, W., Ju, X., Xu, Y., Lu, X., Tian, H., Shi, L., & Shu, G. (2023). Integrating engine thermal management into waste heat recovery under steady-state design and dynamic off-design conditions. *Energy,* 272, article number 127145. doi: 10.1016/j.energy.2023.127145.

[19] Lu, P., Gao, Q., Lv, L., Xue, X., & Wang, Y. (2019). Numerical calculation method of model predictive control for integrated vehicle thermal management based on underhood coupling thermal transmission. *Energies*, 12(2), article number 259. doi: 10.3390/en12020259.

[20] Menter, F.R. (1994). Two-equation eddy-viscosity turbulence models for engineering applications. *AIAA Journal,* 32(8), 1598-1605. doi: 10.2514/3.12149.

[21] Naderi, A., Qasemian, A., Shojaeefard, M.H., Samiezadeh, S., Younesi, M., Sohani, A., & Hoseinzadeh, S. (2021). A smart load-speed sensitive cooling map to have a high-performance thermal management system in an internal combustion engine. *Energy,* 229, article number 120667. doi: 10.1016/j.energy.2021.120667.

[22] Nahliuk, M., Pavlenko, V., Kuzhel, V., & Chernenko, P. (2023). Quality indicators of antifreeze and their correlation with electrical conductivity during the intercity buses operation. *Journal of Mechanical Engineering and Transport*, 17(1), 108-113. doi: 10.31649/2413-4503-2023-17-1-108-113.

[23] Pandey, A., Schlautman, J., Liu, Z., Dhar, S., & Yashwanth, B.L. (2024). Conjugate heat transfer analysis of an i-4 engine including pistons, liners, block, heads, water cooling jacket, and oil cooling jets. *SAE Technical Paper*. doi: 10.4271/2024-01-2696.

[24] Pimpinella, L., Mikuláš, O., Ko, M.S., Bae, I.H., Herceg, M., Pekař, J., Kim, Y.K., & Jung, Y.H. (2021). Advanced coolant temperature control study with integrated thermal management system valve. *IFAC-PapersOnLine,* 54(6), 200-205. doi: 10.1016/j.ifacol.2021.08.545.

[25] Pohorletsky, D.S., Gritsuk, I.V., Khudiakov, I.V., Chernenko, V.V., & Polishuk, A.V. (2023). Features of low-temperature corrosion protection of cylinder sleeves of ship low-speed engines. *Reporter of the Priazovskyi State Technical University. Section: Technical Sciences*, 46, 122-130. doi: 10.31498/2225-6733.46.2023.288181.

[26] Primary Foundry Alloys. (n.d.). *Technical data sheet: AlSi7Mg0.3.* Retrieved from https://cdn.thomasnet.com/ccp/00176659/102129.pdf.

[27] Pylyov, V.V., Linkov, O.Y., & Marchenko, A.P. (2024). Refining the empirical model of the heat transfer boundary conditions of the piston of a high-speed diesel engine. *Internal Combustion Engines,* 2, 3-11. doi: 10.20998/0419-8719.2024.2.01.

[28] Qin, S., Xie, C., Li, S., Yang, Q., Chen, J., & Sun, K. (2022). CFD analysis and optimization of a diesel engine cooling water jacket. *Fluid Dynamics & Materials Processing*, 18(3), 647-659. doi: 10.32604/fdmp.2022.017519.

[29] Salehi, H., Savaripour, H., Bidhendi, H.M.M., Farhani, F., & Rosen, M.A. (2023). Experimental and simulation study of an automobile cooling system: Performance improvement using passive flow control. *International Communications in Heat and Mass Transfer,* 149, article number 107168. doi: 10.1016/j.icheatmasstransfer.2023.107168.

[30] Savaripour, H., Hosseini, S.A., Nasrollahnezhad, S., Jahangiri, A., & Rosen, M.A. (2022). Investigation of engine's thermal management based on the characteristics of a map-controlled thermostat. *International Communications in Heat and Mass Transfer,* 135, article number 106156. doi: 10.1016/j.icheatmasstransfer.2022.106156.

[31] Sheikhi, A., Saray, R.K., Ghazani, A.S., Geimechi, A., & Lashkarpour, S.M. (2026). Thermal management and optimization of a 6-cylinder heavy-duty diesel engine: A two-way coupled CFD, FEA and combustion numerical study. *Fuel*, 405(C), article number 136634. doi: 10.1016/j.fuel.2025.136634.

[32] Tan, L., Yuan, Y., & Huang, C. (2023). CFD modelling on flow field characteristics of engine cooling water jacket and its cooling performance improvement based on coolant transport path analysis method. *Proceedings of the Institution of Mechanical Engineers, Part A: Journal of Power and Energy*, 237(2), 385-401. doi: 10.1177/09576509221116503.

[33] Turabimana, M., Sohn, J.W., & Choi, S.-B. (2023). A novel active cooling system for internal combustion engine using shape memory alloy based thermostat. *Sensors*, 23(8), article number 3972. doi: 10.3390/s23083972.

[34] Yang, L., Lu, G., & Wang, T. (2024). Structure improvement of two-cylinder engine cooling water jacket based on flow field simulation. *Sustainability*, 16(24), article number 11092. doi: 10.3390/su162411092.

[35] Zou, Y., Li, R., Pan, H., Sun, X., & Fu, J. (2025). Performance prediction of electronic fan and water pump of engine cooling system based on joint simulation and machine learning. *Scientific Reports,* 15, article number 15672. doi: 10.1038/s41598-025-00313-x.

Віктор Дуганець
Доктор педагогічних наук, професор
Заклад вищої освіти «Подільський державний університет»
32316, вул. Шевченка, 12, м. Кам'янець-Подільський, Україна
https://orcid.org/0000-0002-3383-5907

Олександр Говоров
Кандидат технічних наук, старший науковий співробітник
Заклад вищої освіти «Подільський державний університет»
32316, вул. Шевченка, 12, м. Кам'янець-Подільський, Україна
https://orcid.org/0000-0002-1645-1725

Віталій Пукас
Кандидат технічних наук, доцент
Заклад вищої освіти «Подільський державний університет»
32316, вул. Шевченка, 12, м. Кам'янець-Подільський, Україна
https://orcid.org/0000-0002-0083-7359

Аналіз та оптимізація систем охолодження двигунів внутрішнього згоряння для підвищення теплової ефективності та надійності роботи двигуна

Анотація. Метою дослідження було кількісно оцінити та оптимізувати роботу систем охолодження двигуна внутрішнього згоряння з огляду на підвищення його теплової ефективності та надійності. Методологія поєднувала моторно-стендові випробування з вимірюванням температур, витрати охолоджувальної рідини та палива, розрахунок теплового потоку з оцінкою невизначеності відповідно до керівництва з вираження невизначеності вимірювань, обчислювальну гідродинаміку у спряженій постановці «рідина – тверде тіло», аналіз напружено-деформованого стану головки блока та дослідження перехідного режиму прогріву від 20 до 90°C. Установлено, що модернізовані конфігурації забезпечили зростання теплового потоку за умов максимального навантаження на 10-17 %, зниження пікових температур у критичних прикамерних зонах на 5-6 % і 10-12 %, а також зменшення внутрішніх температурних градієнтів на 18-22 % і 30-35 %. Це супроводжувалося зниженням еквівалентних напружень на 18-22 % та підвищенням коефіцієнта запасу міцності з 1,45 до 1,87 у найбільш ефективній конфігурації. У перехідному режимі система з електроприводним насосом скорочувала час досягнення робочої температури на 9-12 % і зменшувала інтегральну витрату палива на 10-12 %, тоді як конфігурація з розділеними контурами забезпечувала стабільне зниження цих показників на 6-8 % і 5-7 %, відповідно. Аналіз гальмової питомої витрати палива в контрольних стаціонарних режимах не виявив статистично значущого погіршення паливної економічності для модернізованих систем. Інтегральне ранжування показало, що система з розділеними контурами забезпечує збалансоване поєднання зниження максимальної температури, мінімізації температурних градієнтів і підвищення запасу міцності без компромісів щодо паливної ефективності, тоді як електроприводна помпа є доцільною для мінімізації тривалості прогріву та витрати палива під час холодного запуску. Практична значущість дослідження полягає у формуванні кількісно обґрунтованих критеріїв вибору конфігурації системи охолодження та стратегій керування витратою теплоносія для інженерних підрозділів з метою підвищення теплової надійності й довговічності двигунів

Ключові слова: локальні температурні градієнти; термонапружений стан; еквівалентні напруження; коефіцієнт запасу міцності; перехідний режим прогріву; інтегральна витрата палива